Intratumoral Distribution of Tritiated Fluorodeoxyglucose in Breast Carcinoma: I. Are Inflammatory Cells Important?

Raya S. Brown, Jennifer Y. Leung, Susan J. Fisher, Kirk A. Frey, Stephen P. Ethier and Richard L. Wahl

Division of Nuclear Medicine, Department of Internal Medicine, Department of Radiology, Department of Neurology and the Mental Health Research Institute and Department of Radiation Oncology, The University of Michigan Medical Center, Ann Arbor, Michigan

To investigate the contribution of various tumor components to tumor [^{3}H]FDG uptake, the size of proliferative cell and macrophage populations and the extent of necrosis, inflammatory infiltration and granulation tissue formation were evaluated in syngeneic rat mammary cancers (RMC) grown in immunocompetent rats, an animal tumor model that closely mimics human breast carcinoma. **Methods:** Tissue components of breast cancers grown in female Lewis rats (n=6) were identified histologically and immunohistochemically. Tracer uptake was studied by quantitative autoradiography 2 hr after an intravenous injection of 100 μCi [^{3}H]FDG. **Results:** RMC tumors were glandular, with small foci of necrosis and were surrounded by a thin layer of granulation tissue. Tumors retained approximately 4% of the injected FDG dose (1.9 ± 0.27 μCi/g). Macrophages numbered 0.5% of total cancer cells (1.2 ± 1.0 of 246 ± 77) and 18.0% ± 3.9% of the nuclei of cancer cells were proliferating cell nuclear antigen (PCNA) positive (52 ± 27 of 293 ± 55). FDG uptake (in apparent disintegrations per minute per microgram of protein) in the cancer cell was 47.3 ± 5.6, with the highest uptake in foci of high tumor cell density (82.1 ± 6.3). Lower levels of FDG uptake were found in necrotic areas (19.8 ± 22.9), granulation tissue (26.9 ± 9.2) and areas of inflammatory infiltration (20.5 ± 15.5). **Conclusion:** These data suggest that FDG-PET imaging of untreated breast cancer mainly reflects tracer uptake in cancer cells.

Key Words: breast carcinoma; quantitative autoradiography; tritiated fluorodeoxyglucose; histochemistry

J Nucl Med 1995; 36:1854–1861

Glucose utilization and the uptake of glucose or of glucose analogs are higher in many tumors compared with normal tissues (*1–3*). This increased rate of glucose metabolism is used to distinguish between neoplastic and normal tissues in PET imaging with the [^{18}F]-labeled glucose analog, 2-fluoro-2-deoxy-D-glucose (FDG), as the radiotracer. In patients with breast cancer (*4–6*), and in those with a variety of other human cancers (*7–9*), FDG PET imaging is a powerful noninvasive diagnostic and prognostic tool. Questions concerning the principal tumor sites of FDG uptake and the biologic and/or clinical significance of the high rate of FDG uptake and retention, however, are still not completely resolved. Attempts to correlate the FDG uptake of cancers to their pathologic grade (*10,11*), their proliferative activity (*12*) or their growth rate (*7*) did not produce conclusive results.

Studies of FDG uptake by human ovarian adenocarcinoma cells (*13*) and in human head and neck carcinoma cells lines (*14*) in vitro show strong correlation between the uptake and the number of viable cancer cells in culture, but not with ^{3}H-thymidine uptake or DNA content per 10^5 viable cells. In vivo, other tumor elements, such as the extent of necrosis, the degree of fibrosis and vascularization, blood flow into the tumor mass, infiltration by inflammatory cells and the presence of phagocytes may modify FDG uptake by the tumor, either by limitation of the availability of the glucose analog or by competition for it. Indeed, results from autoradiographic (ARG) studies of FDG uptake in animal tumor models suggest significant FDG uptake by noncancerous components of the tumors, in some cases more than in the cancer cells (*15*), as a result of lower rate of FDG uptake by tumor cells compared with phagocytes and granulation tissue (*16,17*). Conversely, ARG study of xenografts of human ovarian carcinoma grown in nude mice showed FDG uptake in viable tumor cells and no uptake by inflammatory cells or necrotic foci and suggested increased accumulation in living (possibly hypoxic) tumor cells that surround necrotic foci (*18*).

To address the issue of FDG uptake by the nonmalignant components of tumors, FDG uptake in several histologic areas was examined, and the sizes of macrophage and proliferating cell populations and the intratumoral distribution of these cells were studied in solid tumors of syngeneic carcinogen-induced rat mammary carcinoma (RMC) cell line (1–9 RMT) (*19*). These mammary tumors, which were grown in immunocompetent Lewis rats, closely model human breast carcinoma. The intratumoral distribution and

Received Sept. 28, 1994; revision accepted Feb. 14, 1995.
For correspondence or reprints contact: Richard L. Wahl, MD, Division of Nuclear Medicine, University of Michigan Medical Center, 1500 E. Medical Center Dr., B1G 412, Ann Arbor, MI 48109-0028.

the variations in the levels of FDG uptake were assessed from autoradiographs of frozen sections. The distribution and the size of the macrophage population, the relative proportion of proliferating cancer cells and the extent of inflammatory infiltration and granulation tissue formation in these tumors were qualitatively and quantitatively studied in histologic sections with specific immunologic markers. The relative significance of these parameters to the tumor FDG uptake was evaluated.

MATERIALS AND METHODS

Animals

Six female Lewis rats were injected with 1×10^6 transplantable rat mammary tumor cells 1-9 RMT (*19*) into the interscapular fat pad. When the size of the tumors reached about 1 to 2 cm in diameter (about 6 wk postinoculation), the animals were fasted overnight, five of them were injected intravenously with 100 μCi of deoxy-2-fluoro-D-glucose 2 (5,6-[^{3}H]) ([^{3}H]FDG) in 0.2 ml saline, and one animal was injected with 0.2 ml saline (control animal for the autoradiography to rule out chemography). The tumors were removed 2 hr postinjection to ensure high tumor-to-background ratios (*20*). Each tumor was divided into two equal parts: one part was frozen in isopentane (2-methylbutane), cooled in liquid nitrogen and stored at −70°C; the second part was fixed overnight in buffered formalin at 4°C and embedded in paraffin. Two small samples (133 ± 10 mg) from each tumor were used to measure [^{3}H]FDG uptake.

The tumors weighed 2.2 ± 0.9 g and retained 1.9% ± 0.27% of the injected dose per gram (ID/g), as calculated by beta counts of tumor tissue samples that were solubilized by incubation in 8:2 Soluene-350:water for 4 hr at 40°C (according to manufacturer's suggestions, Packard Instrument Co., Meriden, CT). Total uptake by the tumors was about 4% of the injected dose. The uptake in the kidney at the same time was 0.36% ID/g. In tumor samples taken from additional animals (n=2) at 2 hr postinjection of 100 μCi ^{18}FDG (>3,000 Ci/mmole) (*5*) in 0.2 ml of saline and counted in a gamma counter, the uptake was 1.25% ID/g, and the total uptake/tumor was about 10% of the injected dose (tumors were larger than in the experimental group).

Antibodies

Proliferating cells were identified by their binding of a monoclonal mouse antiproliferating cell nuclear antigen (PCNA), PC10 (Dako Corp., Carpinteria, CA). This monoclonal antibody recognizes a 36-kD PCNA (*21-23*) and reacts with nuclei of a wide range of normal and neoplastic cells (*24*). This marker was used to estimate the number of proliferative cells in these tumors. Macrophages were identified by their binding of a monoclonal mouse anti-rat CD11b, 1B6 (kindly provided by R.F. Todd, MD, Internal Medicine, University of Michigan), which specifically reacts with the rat homolog of human Mol/Mac-1 (*25*).

Immunohistochemistry

The binding patterns of the antibodies in the RMC tumors were studied by the avidin-biotin conjugate immunoperoxidase procedure with the Vectastain Elite kit (Vector, Burlingame, CA) (*26*). The nonspecific binding of the secondary antibody, a horse anti-mouse IgG, in fresh frozen sections or in formalin-fixed frozen sections from rat tissues was very high, which resulted in high background staining. The background hindered the discrimination between positive and negative cells. Therefore, paraffin sections of the tumors which provide superior anatomic detail were used for immunostaining.

To identify PCNA-positive cells, paraffin sections were incubated with PC10 diluted 1:50 in a solution of 1% normal horse serum and 4% bovine serum albumin in phosphate-buffered saline (PBS) and stained as above. Slides incubated with hybridoma medium or normal mouse IgG (10 μg/ml of the same diluent as the antibody) were used as negative controls, and paraffin sections of small intestine from a normal fasted rat were used as positive controls.

To identify macrophages, paraffin sections were incubated with 1B6 diluted 1:25 with a solution of 1% normal horse serum and 4% bovine serum albumin in PBS and stained as above. Sections incubated with normal mouse IgG were used as negative controls. Lymph nodes from the axilla of an untreated rat bearing RMC were used as positive controls.

All the stainings were performed at room temperature, and the immunostained slides were lightly counterstained with hematoxylin and examined by light microscopy.

Estimates of Antigen-Positive Cells

Fields to be counted were selected randomly (n=10/tumor). Each section was divided into 2 × 2-mm squares, and one central 400× field was counted in each of 10 randomly chosen squares. The percentage of positive cells was calculated for each tumor.

Autoradiography

Sets of three consecutive 16-μm thick frozen sections, sectioned at intervals of 800 μm through the frozen part of the tumor, were collected on frozen slides (−20°C) and quickly dried on a hot plate to minimize diffusion. Sectioning at 16 μm reduced the chance of distortion and folding of the frozen sections and lessened the variations in section thickness. In studies of autoradiography with tritium at the light microscopic level, mostly beta particles that originate in the upper 1 μm of a section can reach the emulsion, and therefore such autoradiography is largely independent of the section's thickness (*27*). It was assumed that this was also true for macroautoradiography. Moreover, the drying reduced the actual thickness of the fresh frozen sections (up to 80%; average water content of soft tissues), decreased the variations in attenuation caused by differences in tissue thickness between the different histologic areas and the use of the ^{3}H-hyperfilm increased the efficiency of recording (*28*). The dried sections and a set of calibrated plastic standards [12 plastic standards with a 1000-fold range of ^{14}C concentrations for which the relationship between the exposure produced by ^{3}H in brain tissue and that produced by the ^{14}C plastic standards is known (*29*)] were placed in x-ray cassettes and were apposed to hyperfilm-^{3}H at room temperature for 29 days. The films were developed in Kodak D-19 developer (Eastman Kodak, Rochester, NY), full strength, for 4 min, dipped in 1% acetic acid and fixed in Kodak rapid fixer. The histologic structures in each set of sections were identified from the first section on each of the autoradiographed slides that were stained with hematoxylin and eosin (H&E) at the end of the exposure period. Frozen sections of tumor from an untreated animal and kidney tissue from a treated animal were used as controls.

Densitometry

Differences in relative FDG uptake in the various histologic regions of each tumor were estimated from the variations in the relative optical densities of the autoradiographic film images. Histologic areas that were large enough to be recognized macroscopically on

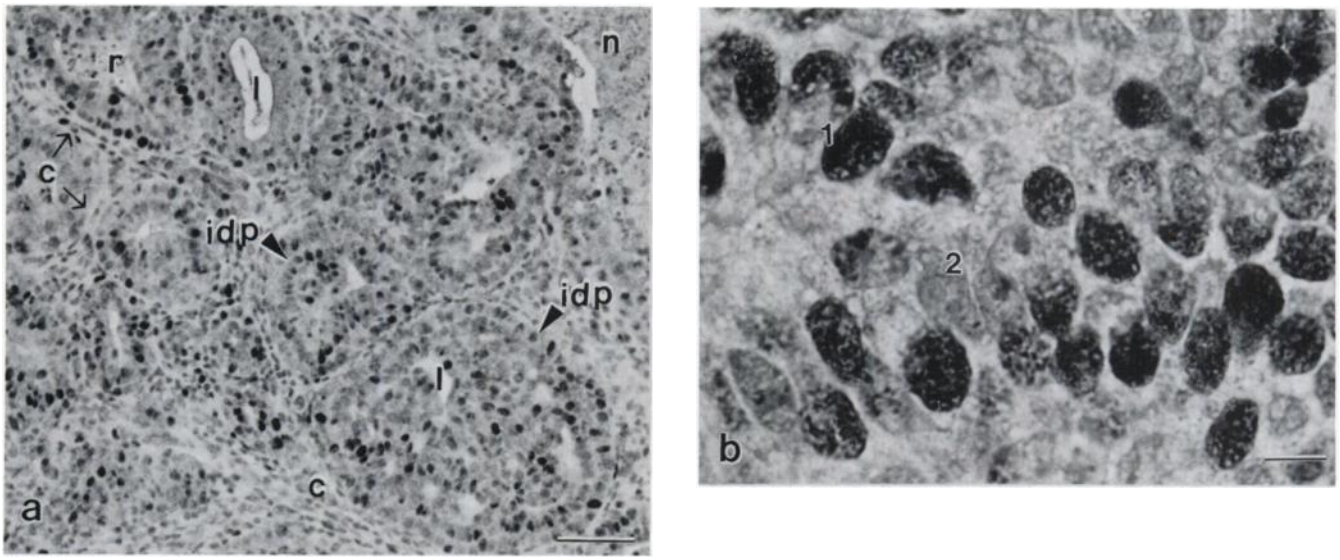

FIGURE 1. Photomicrograph of paraffin section from RMC tumor 2 (T2) grown on syngeneic rat. Section was incubated with PC10 to identify PCNA-positive nuclei. (a) View of area from the margin of the tumor. Cross-sections of several ducts separated from each other by thin ridges of connective tissue (c) are present. Marked intraductal proliferation (idp) is seen, lumens (1) are small, and they sometimes contain necrotic debris (n) (×200, bar=50 μm). (b) Intensity of nuclear staining is heterogeneous. Some nuclei (1) are strongly stained, and some were not stained at all (2) (×800, bar=10 μm).

the H&E-stained sections (about 1 mm^2 or larger in total of 36 cross sections of the tumors) were measured. Each area was examined microscopically and categorized by its predominant histologic characteristic as either a region of densely packed cancer cells, necrosis, inflammatory infiltration or granulation tissue/fibrosis. The borders of each area were traced on the computerized images of the H&E-stained sections and then superimposed on the matching computerized autoradiographic images (three consecutive images per slide, at several depths of the tumors). The numeric estimates of activity in the chosen areas were measured using a computer-assisted video densitometry system (MCID system, Imaging Research Inc., St. Catherine's, Ontario, Canada) (*29*). The relative densities were expressed as apparent disintegrations per minute per microgram (dpm/μg) of protein, according to the calibrated standards. The values measured from the autoradiograms ranged between 1 and 150 apparent dpm/μg protein and were below the grain density saturation of the film, namely relative densities of 0.106 to 0.570 on a scale of 0 to 1 (maximum − minimum film transparency). Biases caused by attenuation from differences in tissue density between brain tissue and tumor tissue or between the different histologic categories of the tumor were negligible.

RESULTS

Histology of RMC Tumors

The tumors were glandular in structure, with mostly empty narrow lumens and occasional dilated ducts, which contained an amorphous substance and infiltrating cells. The tumor cells were organized partly as a monolayer along a thin connective tissue stroma and partly as multilayered intraductal protrusions (cribiform and comedocarcinoma patterns) that often completely filled the lumens and formed solid aggregates of densely packed cells. The cuboidal to columnar epithelial cells were morphologically uniform and had large nuclei. Foci of necrosis, often infiltrated by inflammatory cells and an occasional macrophage, were generally small and most of them were microscopic in size. The tumors were surrounded by a thin layer of granulation tissue (Figs. 1, 3). The granulation tissue, and often the connective tissue stroma, contained numerous microscopic nests of cancer cells.

Immunohistochemistry

Expression of PCNA in RMC Tumors. PCNA-positive nuclei were seen in all six tumors studied. More positive nuclei were found in the periphery of the tumor mass than in its center. The intensity of the nuclear staining was heterogeneous, with variations from area to area and between tumors. The nuclear staining was granular in most cases (Fig. 1), and in some cells the cytoplasm was also stained (results not shown). The average proportion of PCNA-positive nuclei in these tumors was 17.8%, with a range of 11.4% to 23.0% (Table 1). No correlation was found between FDG uptake and the number of PCNA-positive nuclei ($r=0.1$; $p=0.4$). In the small intestine control, positive nuclei were limited to the crypts, as expected (*24*), and no staining was observed in sections of either the tumor or the intestine that were incubated with hybridoma supernatant that contained 15% to 20% fetal calf serum or with normal mouse IgG instead of the primary antibody.

Distribution of Macrophages in RMC. CD11b-positive cells with macrophage morphology (large, vacuolated cells with small nuclei) (Fig. 2) were seen in all of the tumors studied. Cancer cells and cell debris in the necrotic lesions were CD11b negative. These CD11b-positive macrophages were sometimes grouped in clusters, but they did not appear to be associated with any specific histologic structure. The largest clusters of macrophages were frequently, but not exclusively, seen near necrotic areas. In some areas of some of the tumors, many CD11b-positive macrophages

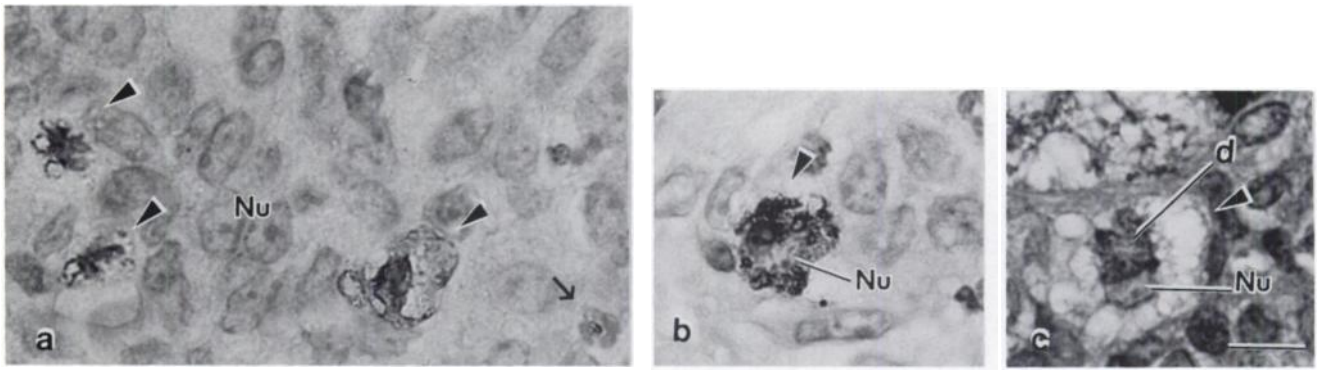

FIGURE 2. Macrophages in paraffin sections from RMC tumor 3 (T3) grown on syngeneic rat. Sections in (a) and (b) were incubated with 1B6 to identify macrophages. Section in (c) was stained with periodic acid-Schiff and counterstained with hematoxylin (*30*) (×1000; bar=10 μm). (a) Several macrophages with CD11b-positive membranes and granules (arrowheads) are seen among viable cancer cells. (b) CD11b-positive macrophage (arrowhead). CD11b-positive granules are seen in cytoplasm of macrophage. Note kidney-shaped nucleus (Nu). (c) Active macrophage containing nuclear debris from cancer cells (arrowhead). In this tumor notice macrophage size compared with average size of cancer cell, kidney-shaped nucleus (Nu) and cytoplasmic vacuoles typical of macrophages. Arrow identifies an infiltrating polymorphonuclear leukocyte.

were seen, although only few or none were found in others. Although CD11b-positive cells were seen inside necrotic areas, the clusters of the CD11b-positive macrophages were mostly seen among viable cells. These clusters contained 2-78 positive cells when among viable tumor cells (mean 33.1±21.6) and 1-22 positive cells in necrotic areas (mean 9.4±8.0). The CD11b-positive cells constituted about 0.5% (1.2±1.0 of 254±45) of the tumor cells (Table 1). A few small cells with CD11b-positive cytoplasmic granules were sometimes seen among infiltrating leukocytes in and/or around necrotic areas. Very few cells with monocyte/macrophage morphology were seen in the thin layer of granulation tissue that surrounded the tumors, and they were CD11b negative. No correlation was found between FDG uptake and the number of macrophages present in this tumor.

In the axillary lymph nodes (no evidence of lymph node metastasis was observed), macrophages and some monocytes, mostly in the sinuses, but sometimes also among lymphocytes in other areas, contained CD11b-positive grains. Some CD11b-positive neutrophils were also observed. Sections of tumors or lymph nodes that were incubated with mouse IgG (10 μg/ml) instead of the IB6 were negative.

Autoradiography

Autoradiographic images of areas of viable cancer cells were darker than areas that corresponded to primarily granulation tissue or the discernible necrotic areas (Fig. 4). The darkest areas (high FDG uptake) in the autoradiograms corresponded to regions of highest viable cancer cell density (areas with marked intraductal proliferation). Granulation tissue, inflammatory infiltration and necrosis were associated with low levels of FDG uptake (Table 2). The levels of FDG uptake in regions with high cancer cell density were 3–4 fold higher than that of granulation/fibrotic tissue regions of the same tumor. High levels of

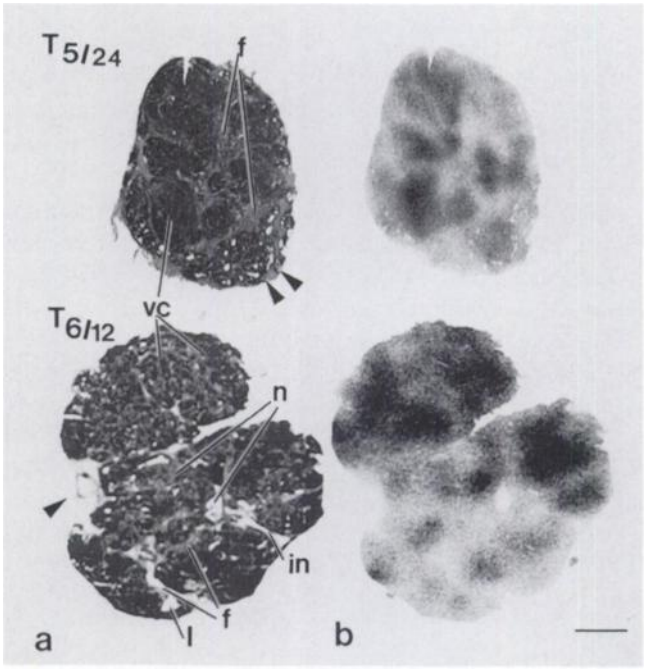

FIGURE 3. FDG uptake in sections from RMC tumors grown on syngeneic rat (from tumor 5, slide T5/24 and from tumor 6, slide T6/12). (a) Sections from tumor 5 (T5/24, left top) and tumor 6 (T6/12, left bottom) stained with H&E. (b) Autoradiograms of same sections, T5/24 (right top) and T6/12 (right bottom). Note marked differences in the histology and FDG uptakes between the two tumors and considerable intratumoral variations in FDG uptake in T6. In section T5/24, 25% of the area was taken up by granulation and fibrotic tissues (f). Regions of high FDG uptake in autoradiogram (average uptake 84.3 apparent dpm/μg protein) correspond to areas of high tumor cellularity (vc); FDG uptake in the large lumens (l) and low cell density (double arrowheads) was lower (average uptake 50.1 apparent dpm/μg protein). The few necrotic sites present in this tumor were microscopic in size and could not be identified on H&E image.

TABLE 1
Relationships between Tritiated Fluorodeoxyglucose Uptake and Proliferating Cell Nuclear Antigen-Positive Cells or CD11b-Positive Cells in Syngeneic Rat Mammary Cancer*

	PCNA+ cells†	CD11b+ cells‡	[^{3}H]FDG (μCi/g)
T1	49.2 ± 18.4 (19.1 ± 6.9)§	0.7 ± 1.3 (0.30)	Untreated (control)
T2	48.6 ± 28.2 (18.1 ± 11.1)	2.8 ± 2.3 (1.34)	2.16
T3	55.7 ± 35.7 (23.2 ± 11.8)	0.3 ± 0.7 (0.15)	1.53
T4	21.5 ± 12.3 (19.1 ± 6.7)	2.1 ± 2.1 (0.66)	1.69
T5	53.3 ± 32.8 (17.4 ± 10.7)	0.3 ± 0.7 (0.15)	1.90
T6	38.1 ± 6.7 (11.3 ± 1.7)	1.0 ± 1.1 (0.48)	1.86

*PCNA-positive nuclei in cancer cells (proliferating cells) or CD11-positive cells with macrophage morphology (large, vacuolated cells with small nuclei) were counted in 10 fields/slide. Each slide was divided into 2 × 2-mm squares, and one central 400× field was counted in each of the 10 randomly chosen squares.

†Mean ± s.d. The average number of cancer cells/field was 293 ± 55.

‡Not all the fields counted contained CD11+ cells. CD11+ cells were counted in fields with necrotic areas or granulation tissue, which sometimes did not include cancer cells. The average number of cancer cells per field counted was 246 ± 78. The percentage of macrophages was calculated from the sum of macrophages in 10 fields/sum of cancer cells in 10 fields for each tumor.

§Numbers in parentheses indicate percentage of positive nuclei or cells from total nuclei or cells counted per field.

PCNA = proliferating cell nuclear antigen; FDG = fluorodeoxyglucose.

uptake, sometimes as high or higher than the average uptake of the combined viable cancer cell regions, were seen in the small areas of the necrosis/inflammatory infiltration (about 8% of the section's area).

The combined contribution of these two histologic categories to FDG uptake, however, was only about 5% of the total. The calculated average of FDG uptake in areas of viable cancer cells (about 72% of the section area) was about 80% of the total uptake and was 15% in granulation and fibrotic tissue regions (20% of the section area) (Fig. 4). The FDG uptake in kidneys of treated animals was one fifth of that of the tumor tissue (0.36 μCi/g), and coexposure of the film to frozen sections of kidneys produced a diffused image of slightly above background density. Frozen sections of tumor from the untreated animal did not produce any image and therefore ruled out a contribution of chemography to the film density.

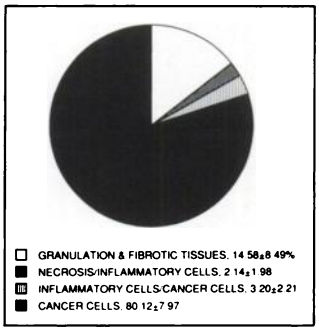

FIGURE 4. Proportion of FDG uptake in the different histologic components in tumors of rat mammary carcinoma grown on syngeneic rats.

DISCUSSION

These results indicate that living cancer cells are the main site of FDG uptake in syngeneic rat mammary tumors in vivo. The contribution of the non-neoplastic components of the tumors to the uptake was about 20% of the total uptake. The numbers of macrophages in these tumors are very small, and the uptake in the granulation and fibrotic tissues, which averaged 20% of the section's area, was 15% of the total.

Macroautoradiography is often used and considered to be a reliable method to compare the distribution of radiolabeled compounds between relatively large areas of structurally complex specimens (*28*). The presence and the amount of the radioactivity is recognized and can be quantified by the degree of blackening of the film. Several factors, such as the energy of beta particles, distance of the source from the emulsion and self-absorption by the specimen or the film used, may affect the grain density obtained in the autoradiogram. When dried frozen sections are used, differences in tissue thickness between different histologic regions may also contribute to the variations in the grain densities. For example, the efficiency of recording over necrotic areas, which are subjected to tissue liquefaction, may be higher compared with areas of densely packed tumor cells because the former dry down to a thinner layer compared with areas of undamaged tissues and the latter might absorb more beta particles. The variations caused by the differences in the densities, self-absorption or the distance of the source from the emulsion between these areas relative to average film densities that were measured over large areas are not significant. These autoradiograms show that the average FDG uptake in areas of either inflammatory infiltrating cells or necrotic tissue is lower than that of areas of cancer cells. These findings, in a mammary tumor grown in an immunocompetent animal, are concordant with those we previously described in HTB77 IP3 human ovarian carcinoma xenografts grown in immunodeficient mice in which FDG uptake was mainly found in viable cancer cells with little uptake in necrotic regions or infiltrating cells (*18*).

These findings are, nevertheless, at variance with data from the tumors of syngeneic FMA3A mammary carcinoma cells and MH13 syngeneic hepatoma cells grown on mice, in which the highest concentration of FDG activity at 1 hr postinjection was in the granulation tissue that surrounded the tumors and in areas rich in macrophages (*15–17*). It is unlikely that the time interval from administration of radioactivity to tumor excision is the source of the discrepancy in the results between the two studies because similar FDG uptake was found in several animal models whether it was measured at 1 or at 2 hr postinjection (*20*); see also Figure 2 in ref. (*17*). This discrepancy could have resulted from differences in the extent of inflammatory cell

TABLE 2
Tritiated Fluorodeoxyglucose Uptake* in the Different Histologic Regions in Syngeneic Rat Mammary Cancer†

Slide no.	Granulation and fibrotic tissues‡	Necrosis/ Inflammatory cells	Inflammatory cells/Cancer cells	Cancer cells/All areas combined§	Cancer cells/Dense areas only¶
2/20 (NL)	36.01 ± 0.64	NL	NL	44.64 ± 0.34	71.86 ± 2.88
3/13 (NL)	35.46 ± 1.73	64.93 ± 2.99	NL	50.63 ± 2.83	86.22 ± 5.10
3/28	33.30 ± 0.90	45.70 ± 1.38	66.81 ± 1.85	50.06 ± 1.08	88.55 ± 1.25
4/12	10.24 ± 0.53	29.19 ± 0.48	8.83 ± 1.23	53.57 ± 1.25	nd
4/23 (NL)	19.02 ± 2.13	—	60.81 ± 2.28	43.66 ± 1.91	84.82 ± 3.85
4/24 (NL)	10.62 ± 0.84	21.87 ± 2.60	NL	42.82 ± 0.89	nd
5/12 (NL)	26.99 ± 1.12	NL	44.07 ± 0.62	51.49 ± 1.89	80.58 ± 1.85
5/23 (NL)	29.30 ± 1.39	NL	58.14 ± 5.28	61.69 ± 10.49	93.35 ± 6.79
5/24 (NL)	27.12 ± 1.97	NL	6.96 ± 1.37	50.82 ± 3.08	84.34 ± 2.10
6/12	6.82 ± 1.61	25.10 ± 0.40	11.68 ± 1.18	31.60 ± 1.01	nd
6/23	27.68 ± 4.44	17.93 ± 5.25	17.56 ± 3.54	44.55 ± 7.54	nd
6/30 (NL)	34.99 ± 4.64	36.98 ± 0.99	NL	44.02 ± 2.77	80.36 ± 6.26

*Mean ± s.d. of three consecutive sections (in apparent disintegrations per minute per microgram of protein).
†FDG uptake was measured by a computer-assisted video densitometer, as described in Materials and Methods.
‡Areas were characterized by their main histologic component. Thus, granulation and fibrotic tissues were dotted with microscopic nests of cancer cells, and many cancer cells were present in areas of inflammatory cell infiltration.
§Section area minus areas of other categories. It consisted of areas dominated by cancer cells but includes some connective tissue stroma and lumens of duct that showed minimal FDG uptake (Fig. 3).
¶Highest uptake in areas with high density of cancer cell.
nd = not determined; NL = area was not large enough to be recognized macroscopically.

infiltration and necrosis and the number of macrophages present in the tumors studied. Similarly, it is possible that the differential relative FDG uptakes in these models are due to differences in the metabolic rates of the cancer cells compared with that of the intratumoral macrophages. Because the differences in the macrophage counts and in their intratumoral localization between these tumors could have solely resulted from the different methods of macrophage identification that were used (morphology compared with a specific antigenic marker), the possibility that the differential FDG uptake may indicate differences in the metabolic rates of the cancer cell lines cannot be ruled out.

The content of macrophages in malignant tumors in humans can vary considerably. Some of these variations may be attributed to the heterogeneity of cancers in general, but difficulties in morphologic identification of macrophages (mainly when histologic sections of carcinomas are counted), error in sampling (mainly when cell suspensions are used) and/or the use of different markers may exacerbate the inherent variability of macrophage content in tumors (*31*). In human breast cancer, for example, estimates of the proportion of cells with macrophage characteristics can range from 0% to 30% (*32*) to 19% to 64% (*31*). Generally, less variation in the number of macrophages and in tumor morphology is observed between tumors in animal models compared with human tumors, but different cell lines grown in different animals may result in tumors that differ considerably from each other. These results clearly show that, in this syngeneic rat mammary tumor, grown in immunocompetent rats, FDG does not accumulate in granulation tissue, and the levels of FDG in areas with necrosis and inflammatory infiltration are below those found in cancer cells. The number of macrophages in these tumors is small, and their contribution to the total tumor uptake is at most minimal.

No correlation between FDG uptake and the proportion of cancer cells with PCNA-positive nuclei was found in this breast cancer animal model. Similarly, no correlation between FDG uptake and proliferating-cell fraction was found in HTB77 IP3 human ovarian carcinoma cells (*13*) or in human head and neck cells (*14*) studied in vitro. The average proportion of PCNA-positive nuclei in the rat mammary tumors varied from 11% to 23% (median of 18.6%); in tissue culture, about 50% of the RMT cells incorporated [^{3}H]thymidine (*unpublished results*). These variations are in the range of those reported for human breast cancer in which the proportions of PCNA-positive nuclei can be as low as 0.7% or as high as 85% (medians of 14.4 or 36%) (*33,34*), depending on the tumor grade or whether the counts were obtained from fields in the most active areas of the sections (e.g., average of 46% PCNA-positive nuclei in the most active areas compared with 29% of all the nuclei in the section; n=205) (*35*) or were randomly selected (average of 6.3%; n=42) (*36*).

There was also a considerable intratumoral heterogeneity in the distribution of the PCNA-positive nuclei, but in general there were more PCNA-positive nuclei in the periphery of the tumor compared with its center. High scores of PCNA-positive nuclei in the periphery of the tumor have been described in human breast cancer (*34*). FDG uptake in the periphery of the rat mammary tumors, in contrast to the number of PCNA-positive nuclei, was lower in most

cases than the FDG uptake in the center of the tumor. No correlation was found between FDG uptake in the syngeneic rat mammary tumors and the percentage or the number of cancer cells with PCNA-positive nuclei.

Immunohistochemical determination of tumor growth fraction with antibodies to cell cycle-associated antigens has been widely used to detect proliferating cells in situ. However, none of the available markers nor any of the other methods to determine proliferation (mitotic figure counts, thymidine or bromodeoxyuridine incorporation or DNA flow cytometry) is free of shortcomings and has gained general acceptance (*37–39*). One of the concerns with the immunodetection of PCNA-positive nuclei in paraffin sections is the possibility that the antigen is masked as a result of fixation and/or embedding (*24*). Additional concerns are:

1. Because of the relative long half-life of PCNA in malignant cells, it may be detected in cells that recently have stopped cycling (*40*)
2. PCNA is overexpressed in cancer cells as a result of aberrant mRNA stability or abnormal expression of growth factors (*41*).

Although noncycling cells can express immunoreactive PCNA and the percentage of PCNA-positive nuclei may be higher than the bromodeoxyuridine labeling index, there is a strong correlation between the two parameters in both normal rat tissues and in growing rat mammary tumors, and therefore PCNA can be used as a marker for the growth fraction in tissues (*24,42*). Moreover, when tumor heterogeneity is a factor, PCNA indices may give a better estimate of proliferating cell populations than flow cytometry because the latter is prone to sampling error (*43*). Thus, the use of PCNA expression as a marker of the tumor-proliferating fraction is a reasonable choice, and the size of the fraction of cancer cells with PCNA-positive nuclei most likely indicates the growth capacity of these syngeneic rat mammary tumors. Lack of correlation between FDG uptake and the growing fraction of cancer cells in the rat mammary tumor is not unique to this tumor and has also been reported in some human cancers (*44*).

In these solid tumors, the autoradiograms show that the highest FDG uptake is found in areas of densely packed viable cancer cells. These findings indicate that FDG uptake in the untreated tumor is mostly dependent on the number of cancer cells present, and high concentrations of the tracer are found in areas of high tumor cellularity. The high correlation between FDG uptake and the number of viable cells found in human adenocarcinoma and squamous cell carcinomas of the head and neck in vitro studies (*13–14*) and the correlation between FDG uptake and tumor cellularity found in patients with recurrent rectal cancer (*45*) support this view. Similar studies to investigate FDG uptake and its distribution in malignant and nonmalignant components of tumors during and/or after treatment could be valuable for understanding cancer biology. The data presented here illustrate the relative contribution of different tumor components to the total FDG uptake in this mammary cancer. Such data provide the necessary baseline for the assessment of treatment-induced changes in FDG uptake, a better understanding of cancer biology and, eventually, a better interpretation of PET FDG images.

CONCLUSION

The results presented in this article show that FDG uptake in this syngeneic breast cancer model depends on tumor cellularity and that 80% of tracer accumulates in viable cancer cells. Conversely, FDG uptake does not seem to be correlated with the proliferating-cell fraction and the contribution of macrophages and inflammatory infiltrating cells to the overall uptake is not substantial. These data suggest that FDG PET of untreated breast cancer images viable cancer cells.

ACKNOWLEDGMENTS

The authors thank Robert F. Todd, Department of Internal Medicine, University of Michigan, for supplying the monoclonal 1B6 anti-CD11b and Tim Desmond, Mental Health Research Institute, University of Michigan, for technical advice. This study was supported by National Cancer Institute grants CA 53172 and CA 52880.

REFERENCES

1. Warburg O. *The metabolism of tumors.* New York: Richard R. Smith Inc.; 1931:29–169.
2. Watanabe A, Tanaka R, Takeda N, Washiyama K. DNA synthesis, blood flow, and glucose utilization in experimental rat brain tumors. *J Neurosurg* 1989;70:86–91.
3. DiChiro G. Positron emission tomography using [^{18}F] fluorodeoxyglucose in brain tumors: a powerful diagnostic and prognostic tool. *Invest Radiol* 1986;22:360–371.
4. Wahl RL, Cody RL, Hutchins GD, Kuhl DE. PET imaging of breast cancer with ^{18}FDG. *Radiology* 1989;173:419.
5. Wahl RL, Cody RL, Hutchins GD, Mudgett EE. Primary and metastatic breast carcinoma: initial clinical evaluation with PET with the radiolabeled glucose analogue 2-[F-18]-fluoro-2-deoxy-D-glucose. *Radiology* 1991;179: 765–770.
6. Kubota K, Matsuzawa T, Amemiya A, et al. Imaging of breast cancer with [^{18}F] fluorodeoxyglucose and positron emission tomography. *J Comput Assist Tomogr* 1989;13:1097–1098.
7. Strauss LG, Conti PS. The application of PET in clinical oncology. *J Nucl Med* 1991;32:623–648.
8. Gupta NC, Frick MP. Clinical application of positron emission tomography in cancer. *CA Cancer J Clin* 1993;43:235–254.
9. Glaspy JA, Hawkins R, Hoh CK, Phelps ME. Use of positron emission tomography in oncology. *Oncology* 1993;7:41–55.
10. DiChiro G, DeLa Paz RL, Brooks RA, et al. Glucose utilization of cerebral gliomas measurements by [^{18}F]fluorodeoxyglucose and positron emission tomography. *Neurology* 1982;32:623–648.
11. Tyler JL, Diksic M, Villemure J-G, et al. Metabolic and hemodynamic evaluation of gliomas using positron emission tomography. *J Nucl Med* 1987;28:1123–1133.
12. Haberkorn U, Strauss LG, Dimitrakopoulou A, et al. PET studies of fluorodeoxyglucose metabolism in patients with recurrent colorectal tumors receiving radiotherapy. *J Nucl Med* 1991;32:1485–1490.
13. Higashi K, Clavo AC, Wahl RL. Does FDG uptake measure proliferative activity of human cancer cells? *In vitro* comparison with DNA flow cytometry and tritiated thymidine uptake. *J Nucl Med* 1993;34:414–419.
14. Minn H, Clavo AC, Wahl RL. In vitro comparison of cell proliferation kinetics and uptake of tritiated 2-fluoro-2-deoxy-D-glucose and L-methionine in squamous cell carcinoma of the head and neck. *J Nucl Med* 1995; 36:252–253.
15. Kubota R, Yamada S, Kubota K, Ishiwata K, Tamahashi N, Ido T. Intratumoral distribution of fluorine-18-fluorodeoxyglucose in vivo: high accu-

mulation in macrophages and granulation tissue studied by microautoradiography. *J Nucl Med* 1992;33:1972–1980.
16. Kubota R, Kubota K, Yamada S, Tamahashi N, Tada M, Ido T. Cellular kinetics of FDG uptake by tumor tissue components *in vivo* studied by microautoradiography. *J Nucl Med* 1993;34:244P.
17. Kubota R, Kubota K, Yamada S, Tada M, Ido T, Tamahashi N. Microautoradiographic study for the differentiation of intratumoral macrophages, granulation tissues and cancer cells by the dynamics of fluorine-18-fluorodeoxyglucose uptake. *J Nucl Med* 1994;35:104–112.
18. Brown RS, Fisher SJ, Wahl RL. Autoradiographic evaluation of intratumoral distribution of 2-deoxy-D-glucose and monoclonal antibodies in xenografts of human ovarian adenocarcinoma. *J Nucl Med* 1993;34:75–82.
19. Ethier SP, Cundiff KC. Importance of extended growth potential and growth factor independence on in-vivo neoplastic potential of rat mammary carcinoma cells. *Cancer Res* 1987;47:5316–5322.
20. Wahl RL, Hutchins GD, Buchsbaum DJ, Liebert M, Grossman HB, Fisher S. Fluorine-18-2-deoxy-2-fluoro-D-glucose uptake into human tumor xenografts. Feasibility studies for cancer imaging with positron-emission tomography. *Cancer* 1991;67:1544–1550.
21. Waseem NH, Lane DP. Monoclonal antibody analysis of the proliferating cell nuclear antigen (PCNA). Structural conservation and the detection of nucleolar form. *J Cell Sci* 1990;96:121–129.
22. Lee SH, Hurwitz J. Mechanism of elongation of primed DNA by DNA polymerase delta, proliferating nuclear antigen and activator 1. *Proc Natl Acad Sci USA* 1990;87:5672–5676.
23. McCormick D, Hall PA. The complexities of proliferating cell nuclear antigen. *Histopathology* 1992;21:591–594.
24. Hall PA, Levison DA, Woods AL, et al. Proliferating cell nuclear antigen (PCNA) immunolocalization in paraffin sections: an index of cell proliferation with evidence of deregulated expression in some neoplasms. *J Pathol* 1990;162:285–294.
25. Mulligan MS, Wilson GP, Todd RF, et al. Roll of beta 1 and beta 2 integrins and ICAM-1 in lung injury after deposition of IgG and IgA immune complexes. *J Immunol* 1993;150:2407–2417.
26. Hsu SM, Rain L, Fanger H. Use of avidin-biotin-peroxidase complex (ABC) in immunoperoxidase techniques: a comparison between ABC and unlabeled antibody (PAP) procedures. *J Histochem Cytochem* 1981;29:577–580.
27. Salpeter MM, Budd GC, Mattimoe S. Resolution in autoradiography using semithin sections. *J Histochem Cytochem* 1974;22:217–222.
28. Rogers AW. *Techniques in autoradiography,* 3rd edition. Amsterdam: Elsevier/North-Holland Medical Press; 1979.
29. Pan HS, Frey KA, Young AB, Penney JB Jr. Changes in [^{3}H]muscimol binding in substantia nigra, entopeduncular nucleus, globus pallidus and thalamus after striatal lesions as demonstrated by qualitative receptor autoradiography. *J Neurosci* 1983;3:1189–1198.
30. Mowry RW. The special value of methods that color both acidic and vicinal hydroxyl groups in the histochemical study of mucins. With revised directions for the colloidal iron stain, the use of Alcian blue G8X and their combinations with the periodic acid-Schiff reaction. *Ann N Y Acad Sci* 1963;106:402–423.
31. Steele RJC, Brown M, Eremin O. Characterization of macrophages infiltrating human mammary carcinomas. *Br J Cancer* 1985;51:135–138.
32. Gauci CL, Alexander P. The macrophage content of some human tumors. *Cancer Lett* 1975;1:29–32.
33. Frierson HF Jr. Immunohistochemical analysis of the proliferating cell nuclear antigen (PCNA) in infiltrating ductal carcinomas: comparison with clinical and pathologic variables. *Mod Pathol* 1993;6:290–294.
34. Siitonen SM, Isola JJ, Rantala IS, Helin HJ. Intratumor variation in cell proliferation in breast carcinoma as determined by antiproliferating cell nuclear antigen monoclonal antibody and automated image analysis. *Am J Clin Pathol* 1993;99:226–231.
35. Aaltomaa S, Lipponen P, Syrjanen K. Proliferating cell nuclear antigen (PCNA) immunolabeling as a prognostic factor in axillary lymph node negative breast cancer. *Anticancer Res* 1993;13:533–538.
36. Magno WB, Hirchfield L, Bhuiya T, Harrison G, Mir R. Correlation of proliferating index (PCNA reactivity and Ki-67 reactivity) in primary breast carcinoma with hormone status, lymph node status, and disease-free survival. *Conn Med* 1992;56:667–669.
37. Hall PA, Levison DA. Assessment of cell proliferation in histological material. *J Clin Pathol* 1990;43:184–192.
38. Quinn CM, Wright NA. The clinical assessment of proliferation and growth in human tumors: evaluation of methods and applications as prognostic variable. *J Pathol* 1990;160:93–102.
39. Kreipe H, Heidebrecht HJ, Hansen S, et al. A new proliferation-associated nuclear antigen detectable in paraffin-embedded tissues by the monoclonal antibody Ki-S1. *Am J Pathol* 1993;142:3–10.
40. Bravo R, MacDonald-Bravo H. Existence of two populations of cyclin/proliferating cell nuclear antigen during the cell cycle: association with DNA replication sites. *J Cell Biol* 1987;105:1549–1554.
41. Chang CD, Ottavio L, Travali S, Lipson KE, Baserga R. Transcriptional and post-transcriptional regulation of the proliferating cell nuclear antigen gene. *Mol Cell Biol* 1990;10:3289–3296.
42. Wijsman JH, Van Dierendonck JH, Keijzer R, Van De Velde CJH, Cornelisse CJ. Immunoreactivity of proliferating cell nuclear antigen compared with bromodeoxyuridine incorporation in normal and neoplastic rat tissue. *J Pathol* 1992;168:75–83.
43. Jain S, Filipe MI, Hall PA, Waseem N, Lane DP, Levison DA. Prognostic value of proliferating cell nuclear antigen in gastric carcinoma. *J Clin Pathol* 1991;44:655–659.
44. Haberkorn U, Strauss LG, Riesser CH, et al. Glucose uptake, perfusion and cell proliferation in head and neck tumors: relation of positron emission tomography to flow cytometry. *J Nucl Med* 1991;32:1548–1555.
45. Ito K, Kato T, Ohta T, et al. Fluorine-18-FDG PET in recurrent rectal cancer: relation to tumor size and cellularity. *J Nucl Med* 1994;35:118.